Optics and Lasers in Engineering 161 (2023) 107338

Contents lists available at ScienceDirect

Optics and Lasers in Engineering

journal homepage: www.elsevier.com/locate/optlaseng

Mutual structure ghost imaging under low sampling

Heyan Huang [a,*], Hang Yang [b], Cheng Zhou [c,e], Lijun Song [d,e,**]

[a] College of Sciences, Shanghai Institute of Technology, Shanghai 201418, China
[b] Changchun Institute of Optics, Fine Mechanics and Physics, Chinese Academy of Science, Changchun 130033, China
[c] School of Physics and College of Chemistry, Northeast Normal University, Changchun 130024, China
[d] Jilin Vocational College of Industry and Technology, Jilin 132013, China
[e] Jilin Engineering Laboratory for Quantum Information Technology, Changchun 130052, China

ARTICLE INFO

Keywords:
Compressed ghost imaging
Low sampling
Mutual structure filtering

ABSTRACT

The realization of high-quality imaging under low sampling is an effective way to solve the practical application of ghost imaging. In this paper, we present an advanced framework of compressed ghost imaging under low sampling. During the imaging process, the regularization and mutual structure filtering operations are performed alternately, which we call mutual structure ghost imaging (MSGI). In the joint filtering of our proposed scheme, the mutual-structural information contained in both the reference image and the target one is applied to enhance the capability of important edge preserving. Thus, high-resolution ghost imaging results can be obtained under low sampling. Moreover, we have adopted a fast-converging iterative format to obtain better imaging results with fewer iterations. Simulation and experimental results show that the proposed method can achieve high-quality imaging results from the random speckle patterns under low sampling and promote the practical process of ghost imaging.

1. Introduction

Ghost imaging (GI) is a novel kind of non-localized imaging which is different from traditional imaging, and it realizes the separation of detection and imaging [1–4]. This new technology has received extensive attention from researchers for its features such as fewer photons, nonlocality, and anti interference. In recent years, GI has been used in nondestructive testing, biological tissue imaging, image optical encryption, medical detection, 3D remote sensing imaging [5–8]. This novel imaging technology has also shown very attractive application prospects in defense and military fields [8,9]. To improve the imaging quality and imaging efficiency of GI, various methods have been proposed, such as iterative GI [10], differential GI [11], compressed GI [12], and so on [13–15]. In particular, the compressed GI shows superiority for the target imaging under low sampling numbers and has great development in image optical encryption, remote sensing imaging, three-dimensional reconstruction, and other practical applications [16–19].

The compressed GI reconstructs image through optimization of a forward model between the scene and image. And, this inverse problem is ill-posed. To obtain a reasonable image estimation, some regularization methods of exploiting the geometrical structure of sparse images need to be utilized. In this paper, we present an advanced framework of compressed ghost imaging based on joint filtering with low sampling numbers. In the imaging process, we perform the regularization and joint filtering operations alternately to reduce the under-sampling noise and improve the quality of a reconstructed image. The joint filtering with mutual structure takes the possible difference between the reference and target images into account, and estimates their mutual structures as a new reference for the joint filtering. This operation can enhance the capability of joint processing in restoring structure based on common information in target and reference images [20]. We introduce this joint filtering in our proposed ghost imaging scheme to enhance the capability of important edge-preserving and obtain high-quality imaging results.

The separate-variable method that decouples regularization and denoising is a commonly used algorithm for solving the reconstruction problems in compressed sensing. So, we alternately perform regularization and mutual structure filtering operations in this paper to solve the ill-conditioned problem in compressed ghost imaging. The proposed scheme has the following benefits: 1) ghost imaging under low sampling: the proposed method can obtain ghost imaging results with fewer sampling numbers, and reduce the detection time; 2) accelerated iteration: in the regularization iterative step, the imaging results can be obtained with fewer iterations by designing a fast-converging iterative format, thereby improving the imaging efficiency; 3) high-quality imaging results: incorporating the mutual structural filtering into a two-step

* Corresponding author.
** Co-corresponding author.
E-mail addresses: huanghy10@mails.jlu.edu.cn (H. Huang), ccdxslj@126.com (L. Song).

https://doi.org/10.1016/j.optlaseng.2022.107338
Received 29 August 2022; Received in revised form 26 September 2022; Accepted 17 October 2022
Available online 29 October 2022

iterative format can improve imaging resolution while removing noise, thereby improving the resolution of ghost imaging.

2. Theoretical analysis

In GI system, the m-th Gaussian random speckle pattern (size $r \times c$) pre-generated by the computer is denoted as $I^{(m)}(x, y)$, and $m = 1, 2, 3, \ldots, M$. Here, M is the total number of sampling. Meanwhile, the object beam illuminates the object with transmission coefficient $O(x, y)$, and the speckle field transmitted by an object is measured with the bucket detector. The detection value obtained from the m-th sampling is recorded as $B^{(m)}$.

Then, each of the speckle intensity $I^{(m)}(x, y)$ is rearranged as a row vector Ψ_m of size $1 \times N$ ($N = r \times c$). After M samples, we get an $M \times N$ matrix A with the following form:

$$A = \begin{bmatrix} \Psi_1 \\ \Psi_2 \\ \vdots \\ \Psi_M \end{bmatrix} = \begin{bmatrix} I_1(1,1) & I_1(1,2) & \ldots & I_1(r,c) \\ I_2(1,1) & I_2(1,2) & \ldots & I_2(r,c) \\ \vdots & \vdots & \ddots & \vdots \\ I_M(1,1) & I_M(1,2) & \ldots & I_M(r,c) \end{bmatrix}. \tag{1}$$

The M detection values from the bucket detector can be permutated into a $M \times 1$ column vector g:

$$g = [B_1, B_2, \ldots, B_M]^T. \tag{2}$$

We rearrange the unknown object $O(x, y)$ as an N-dimensional column vector u ($N \times 1$), then we will have the following framework:

$$g = Au. \tag{3}$$

As we all know, Eq. (3) is a typical mathematical inverse problem due to the interference of environmental noise, background noise, and other noise, and the regularization method is generally used to suppress the noise. A reasonable and effective solution to Eq. (3) can be obtained by solving the following optimization problem:

$$\hat{u} = \arg\min_u \|g - Au\|_2^2 + \lambda \|u\|_{reg}, \tag{4}$$

where, $\|g - Au\|_2^2$ is the fidelity term and $\|u\|_{reg}$ is the regularization term, and $\lambda > 0$ is called the regularization parameter. For the above optimization model Eq. (3), the iterative method is generally used to solve. The core idea of this iterative method is to regard the estimation of the clear image as an optimal solution to the optimization problem and to solve this optimization problem by designing an iterative format to achieve the purpose of image reconstruction.

2.1. Mutual structure ghost imaging

In this paper, we decompose the compressed ghost imaging problem Eq. (3) into two steps of regularization and denoising, and apply an iterative approach to achieve high-quality ghost imaging under low sampling. To improve imaging efficiency, we adopt a fast iterative format to reduce the number of iterations and thus speed up the convergence. The projected Landweber regularization with accelerated iteration and joint filtering with mutual structure are utilized alternately to obtain the imaging results. Fig. 1 shows the flowchart of ghost imaging implementation in this paper. The entire imaging scheme is an iterative process by alternating regularization and denoising steps. Next, we will describe the implementation of our proposed ghost imaging in detail.

Step 1: accelerated projected Landweber iteration

To solve Eq. (3), some effective regularization methods are utilized to get reasonable imaging results, such as Tikhonov regularization, Landweber regularization, and some other iterative methods [21–23]. The projected Landweber iteration regularization (PLIR) [24,25] is easy to implement and has advantages for solving large inverse problems. In particular, this regularization method can get better imaging results in ghost imaging [14,26]. The PLIR format of Eq. (3) is as follows:

$$u_k = u_{k-1} + \beta P A^T (g - A u_{k-1}), \quad k = 1, 2, 3, \ldots, \tag{5}$$

where P is the pseudo-inverse of $A^T A$, β is the parameter that controls the speed of convergence, u_k and u_{k-1} are the current iteration result and the previous iteration result respectively. This projected Landweber result is recorded as $u_k = \text{PLIR}(A, g, u_{k-1})$.

In this paper, we proposed an accelerated projected Landweber iteration (APLIR) inspired by the fast iterative shrinkage-thresholding algorithm (FISTA) [27,28]. The FISTA selects the iteration sequence more smartly, and its iterative process based on the idea of gradient descent approaches the minimum value of the problem more quickly [28]. In our iteration process, we add an intermediate variable υ, and this sequence υ_k is updated by a simple linear combination of the previous two iterations u_{k-1}, u_{k-2}. The specific approximate form is as follows:

$$\begin{cases} t_k = \alpha \frac{1+\sqrt{1+4t_{k-1}^2}}{2} \\ \upsilon_k = u_{k-1} + (\frac{t_{k-1}-1}{t_k})(u_{k-1} - u_{k-2}) \\ u_k = \upsilon_k + \beta P A^T (g - A\upsilon_k). \end{cases} \tag{6}$$

Here, P is the pseudo-inverse of $A^T A$, α is the gain factor to control the error between two consecutive iterations, β is the parameter to decide how much information is obtained from the residual image, t_k is the linear combination parameter, and u_k is the approximate solution of Eq. (3). The initial supposition: $u_0 = u_1 = [0, 0, \ldots, 0]^T$, $t_1 = 1$.

Through the above regularization step, we obtain an initial approximate image u_k with the artifacts and noise introduced by the effect of Eq. (6). This regularization step is recorded as $u_k = \textbf{APLIR}(A, g, u_{k-1}, u_{k-2})$, $k > 1$. To suppress the amplified artifacts and noise introduced in Eq. (6), we apply the joint filtering with mutual structure to denoise image u_k in the following denoising step, and utilize this filtering to obtain high-quality imaging results with few sampling numbers.

Step 2: joint filtering with mutual-structure

By observing the regularization results (shown in Fig. 1), we can find that the initial imaging result obtained by the above regularization contains a lot of noise and the imaging quality is relatively poor. We introduce joint filtering to denoise the regularization result and improve the imaging quality. The mutual structure for joint filtering has shown promising performance in edge-preserving denoising problems. Hence, we integrate it into our ghost imaging scheme for high-quality imaging results.

The mutual structure filtering guides the joint filtering process by finding the mutual structure between the reference image and the target image, and both the target image and reference image are filtered in the filtering process [20]. Thus the resulting image can be enhanced by this joint filtering. In paper [20], the joint filtering measure structure similarity between corresponding patches in filtering output image U and updated reference image G. The result of joint filtering with mutual structure is obtained by minimizing the following objective function for alternately estimating U and G:

$$E(U, G, a, b) = E_S(U, G, a, b) + E_d(U, G) + E_r(a, b), \tag{7}$$

where $E_S(U, G, a, b)$ is the image structure similarity, a and b are regression coefficient sets, which also need to be optimized. The term $E_d(U, G)$ is the regular term to avoid trivial solutions, and the term $E_r(a, b)$ is presented to reduce patch intensity variance, so it can improve the reasonable ability to smooth the target image by removing noise and other visual artifacts [20].

The objective function Eq. (7) is optimized alternatively to get filtering result U and mutual structure G from the initial inputs U_0 and G_0 after reasonable smoothing. In this paper, we denote this joint filtering as $U = \textbf{MSfilter}(U_0, G_0)$. The detailed instructions for the numerical solution of minimizing the objective function Eq. (7) and the source code of mutual structure filtering can be found in the paper [20].

For the ghost imaging scheme proposed in this paper, the resulting image u_k ($N \times 1$) obtained from **step 1** is reshaped into a matrix of $r \times c$ dimensions, then the joint filtering with mutual structure is utilized to

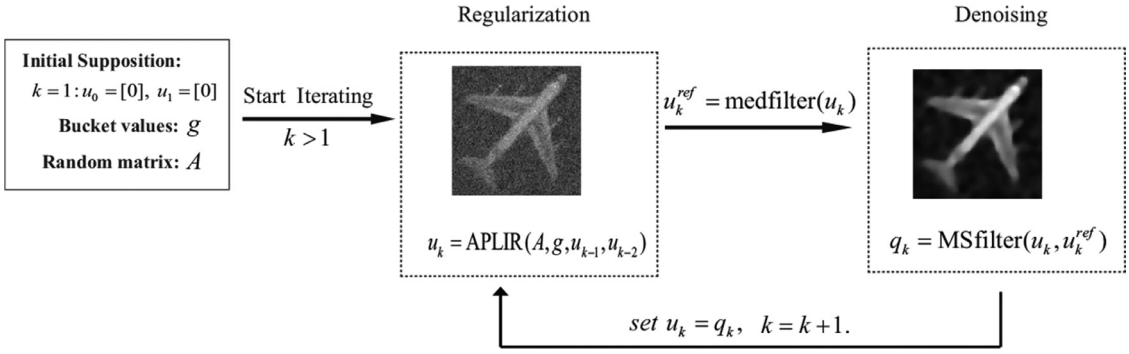

Fig. 1. The flowchart of our proposed ghost imaging.

suppress the amplified noise. Here, we denote this joint filter as

$$q_k = \mathbf{MSfilter}(u_k, u_k^{ref}), \tag{8}$$

where u_k is input image (i.e., the reconstruction result of APLIR), u_k^{ref} is the reference image, which is set as the median filtering result of u_k in our paper to achieve fast convergence [20], q_k is the filtered image.

In the iterative process, we will feed back the filtered results q_k in the next regularization, it makes that the result of regularization not only depend on the speckle matrix A and bucket values g, it is also closer to the result of the previous denoising. By decoupling regularization (**step 1**) and denoising (**step 2**), we alternately perform these two steps iteratively to obtain imaging results. As a result, after repeated iterations in this way, the final converged result can be obtained. The whole ghost imaging algorithm is summarized in Algorithm 1, and is recorded as MSGI in this paper.

Algorithm 1 Mutual structure ghost imaging algorithm.

Input: Bucket values : g, random speckle matrix: A, parameters α, β, the maximum number of iterations $Maxiter$.
1: Initialize: $u_0 = \mathbf{0}$, $u_1 = \mathbf{0}$.
2: for $k = 2{:}Maxiter$ do
3: $u_k = \mathbf{APLIR}(A, g, u_{k-1}, u_{k-2})$
4: $u_k^{ref} = \mathrm{medfilter}(u_k)$
5: Image update: perform the joint filtering: $q_k = \mathbf{MSfilter}(u_k, u_k^{ref})$, and set $u_k = q_k$.
6: end for
Output: Reconstructed image q_k.

3. Result

In this section, we will test the effects of our proposed scheme on different target objects. We demonstrate the performance via numerical simulation and experimental results, and compare our method (MSGI) with the TV-based GI (TVAL3) [29], joint iteration compressed ghost imaging (JIGI) [14,26]. The original images tested in numerical simulation, Gaussian speckle patterns, and imaging results all have resolutions of 128×128 pixels. We select the plane model as the real target object for the actual experiment. In the imaging processing, all the simulations are performed in MATLAB R2013a on an Intel(R) Core i5-8250U 1.6 GHz CPU (one thread used) and 32 GB memory.

In our experimental, α is used to control the error of two adjacent iterations not to be large. If the parameter α is too large, the error information of the iteration will dominate, which will cause the iterative result to contain more noise information, and if the parameter α is set too small, the error information of the two previous iterations will be removed in the iteration, and the imaging result will deviate from the original image. The parameter β controls the speed of convergence and plays an extremely important balancing role in suppressing noise and retaining more effective frequency domain information in the iteration process. We manually adjust the best imaging results, and after many repeated experiments, the value ranges of α and β are respectively set to [0.65, 0.85], [2,5].

3.1. Numerical simulation results

In this section, we measure the imaging quality quantitatively in terms of peak signal-to-noise ratio (PSNR) and structural similarity index (SSIM) [30,31] to objectively evaluate the performance of our proposed method. The PSNR is defined as following:

$$\mathrm{PSNR} = 10\log_{10}\left[\frac{\max Val^2}{\mathrm{MSE}}\right]. \tag{9}$$

Here, $\mathrm{MSE} = \frac{1}{r\times c}\sum_{i=1}^{r}\sum_{j=1}^{c}[u(i,j)-q(i,j)]^2$, and $\max Val$ is the maximum pixel value of an image. The definition of SSIM is as follows:

$$\mathrm{SSIM}(u,q) = \frac{(2\mu_u\mu_q + C_1)(2\sigma_{uq} + C_2)}{(\mu_u^2 + \mu_q^2 + C_1)(\sigma_u^2 + \sigma_q^2 + C_2)}, \tag{10}$$

where u and q represent the original image and the reconstructed image respectively, which have $r \times c$ pixels. μ_u and μ_q are (respectively) the means of u and q, σ_u and σ_q are (respectively) the standard deviations of u and q, and σ_{uq} is the cross-correlation of u and q after removing their means. The terms C_1 and C_2 are small positive constants that stabilize each term. In our paper, we set $C_1 = C_2 = (0.05L)^2$, L is the dynamic range of image pixels, which is set $L = 255$ in our paper. Naturally, the PSNR and SSIM values increase as the quality of reconstructed image becomes better.

Fig. 2 shows simulation results of the "gong" image with TVAL3, JIGI, and MSGI methods under different sampling numbers. By observing Fig. 2, we can find that under the same sampling numbers, our proposed method MSGI can obtain better imaging results compared with TVAL3 and JIGI. When the sampling number is 350 ($M = 350$, the sampling rate is lower than 2.2%), our method MSGI can obtain the overall outline of the object, which indicates the superiority of our ghost imaging under low sampling.

In order to numerically compare these three kinds of ghost imaging results, we also list the PSNR and SSIM values below the corresponding reconstructed images in Fig. 2, which are obtained by different imaging methods with the same sampling numbers. From these values, we can see that, when the number of sampling is less than 550 ($M = 350, 400, 450, 500$), the PSNR values of MSGI are about 4 dB larger than JIGI, and about 6 dB larger than TVAL3, while the SSIM values of MSGI are relatively larger than the other two algorithms. When the number of sampling reaches 550 ($M = 550$), the PSNR and SSIM values obtained by MSGI are still higher than the other two methods. Through the comparison of the results presented in Fig. 2, we can find that our proposed method in this paper can obtain high-quality imaging results under low sampling, both visually and numerically.

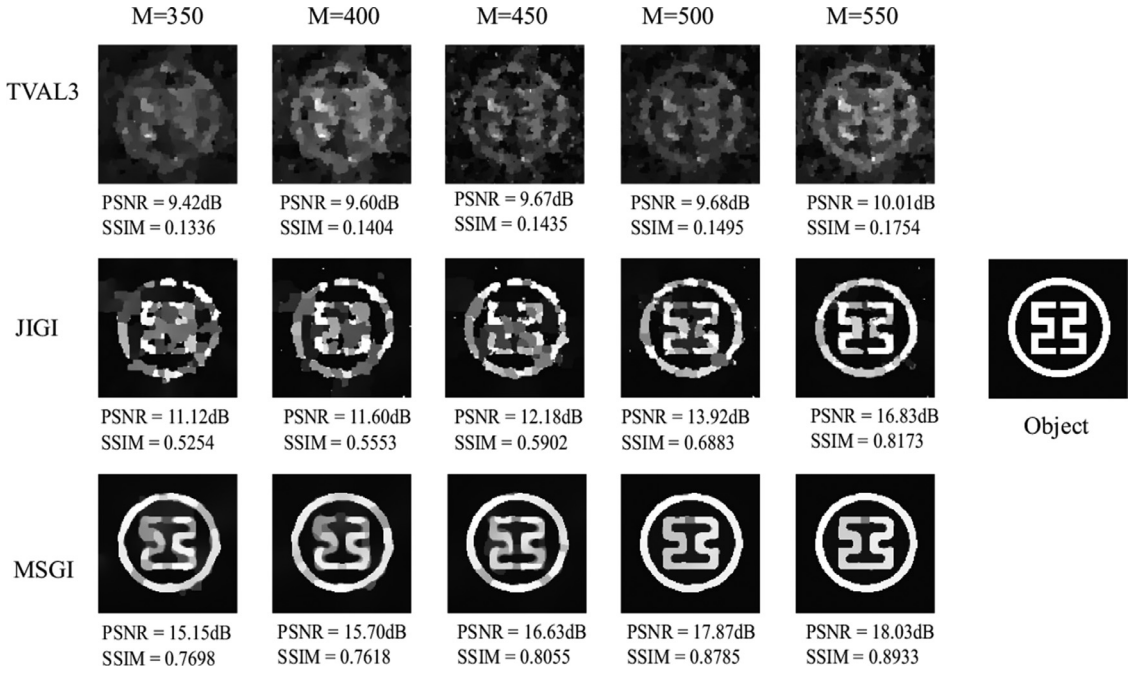

Fig. 2. Simulation results of "gong" image with TVAL3, JIGI and MSGI under M sampling and original object.

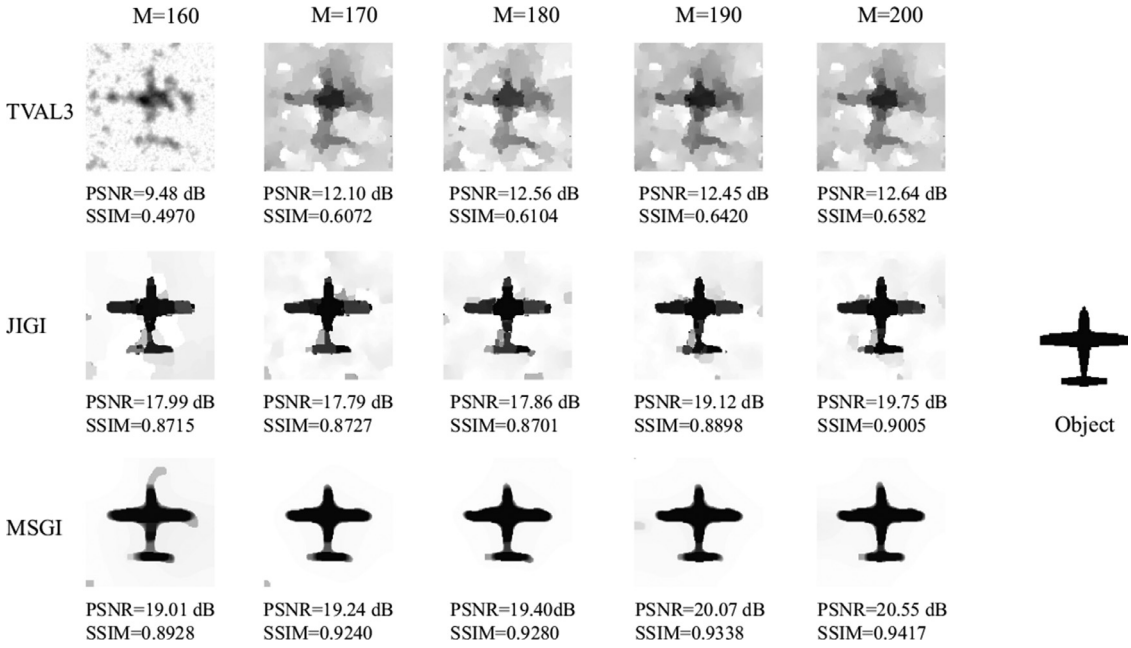

Fig. 3. Simulation results of "aircraft" image with TVAL3, JIGI and MSGI under M sampling and original object.

Fig. 3 shows "aircraft" imaging results of TVAL3, JIGI, and MSGI with different sampling numbers, the PSNR and SSIM values of the reconstructed images are listed below the corresponding results. From this figure, we can see that the images obtained by our proposed method MSGI are clearer and smoother than the other two methods under the same sampling numbers. And, numerical results of MSGI below imaging results are also higher than others. Both the visual and numerical results demonstrate that our method can obtain higher quality imaging results under low sampling numbers. Even at a relatively low sampling number ($M = 200$, the sampling ratio is lower than 1.3%), the imaging result of MSGI is still relatively close to the original images.

To verify the performance of the MSIG scheme under background light noise, we calculate the PSNRs of imaging results under different signal power to the background noise power ratio (DSNR) [26], which is defined as

$$DSNR = 10\log_{10}\frac{\langle B^{(m)}\rangle}{\langle Noise^{(m)}\rangle}, \tag{11}$$

where $\langle B^{(m)}\rangle$, $\langle Noise^{(m)}\rangle$ are the average bucket detection values and average background noise power with m sampling number, respectively. Fig. 4 shows the curve of PSNR with the change of DSNR value when the sampling number is 200 for an "aircraft" object. By looking at the curve, we can find that when different degrees of Gaussian noise are added to the bucket detection values, the PSNR increases as the DSNR increases. And, when DSNR> −10 dB, the PSNR of the imaging results

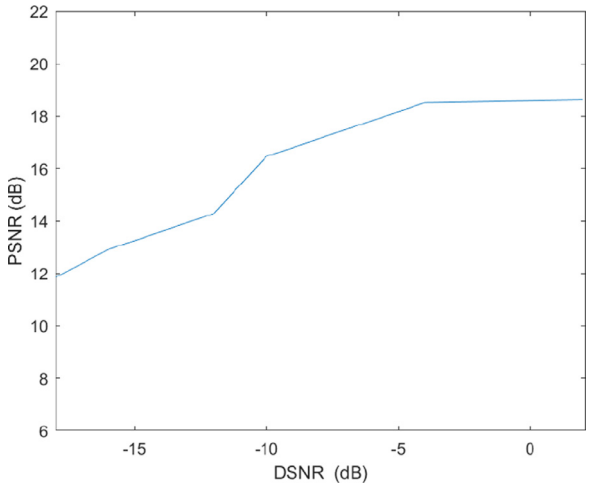

Fig. 4. The PSNR performance of imaging result against DSNR with MSGI method.

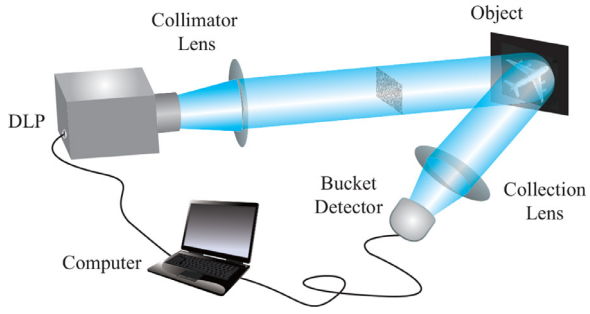

Fig. 5. Experiment schematic diagram of MSGI.

obtained by our method is greater than 16 dB. It shows that the MSGI imaging method has good robustness.

3.2. Experimental results

In this subsection, we conduct the actual experiment to demonstrate the feasibility of MSGI scheme. Fig. 5 shows the schematic of the experimental system. In this experimental system, the Gaussian random speckle matrix is applied to obtain the ghost imaging results. And, the commercial digital light projector (DLP, Hitachi HCP-3050X, 1024×768 pixels with pixel size 12.5×12.5 μm^2, 3000 lumens) is used as the light source to illuminate the object. The object to be imaged is a "plane" printed on the A4 sheet of paper. We select the 128×128 pixels for each random speckle pattern. We collect the reflected signal light with a Si transimpedance amplified photo detector (Thorlabs, PDA100A-EC, 320–1100 nm, 2.4 MHz BW, 100 mm^2).

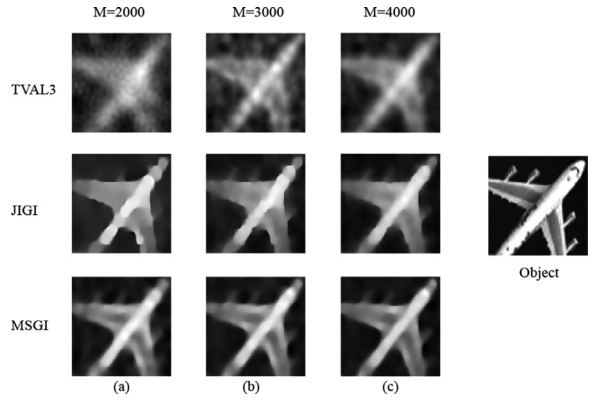

Fig. 7. Enlarged comparison of imaging results of "plane" object with different sampling numbers ($M = 2000$, $M = 3000$, $M = 4000$) and the original enlarged object.

The comparison of imaging results with TVAL3, JIGI, and MSGI under different sampling numbers are shown in Fig. 6. And, in order to see the experimental results of our algorithm more clearly, we have enlarged the part of the experimental "plane" diagram, as shown in Fig. 7.

By observing the experimental results (Fig. 6), we can find that under the same sampling numbers, the MSGI method can obtain better imaging results compared with TVAL3 and JIGI. When the sampling number is low ($M = 500$), our proposed method in this paper can roughly obtain the outline of the object, although there is some blurring of the right-wing and tail (the third row of Fig. 6(a)). When the sampling number rises to 1000 ($M = 1000$, the sampling ratio is about 6.1%), the outline of the entire object has been gradually and completely displayed (the third row of Fig. 6(b)). As the number of sampling increases, some detailed information about the object is gradually reconstructed (the third row of Fig. 6(c) and (d)). Through observation and comparison, we can find that under the same sampling times, the imaging results obtained by MSGI are clearer and the PSNR and SSIM are higher than the other two methods, which can provide strong support for subsequent applications such as accurate identification of targets. The experimental results verify the feasibility of MSGI method proposed in this paper, that is, high-quality imaging results can be obtained under low sampling.

3.3. Accelerated iterative format

In the regularization step, inspired by the fast iterative shrinkage algorithm with backtracking [27,28], we adopt a similar iterative format

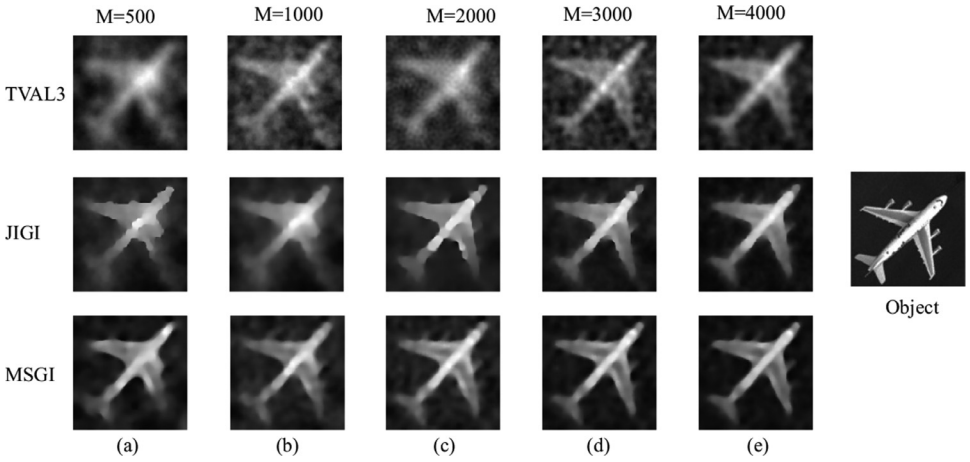

Fig. 6. Experimental reconstructed results of "plane" object with different sampling numbers ($M = 500$, $M = 1000$, $M = 2000$, $M = 3000$, $M = 4000$) and the original object.

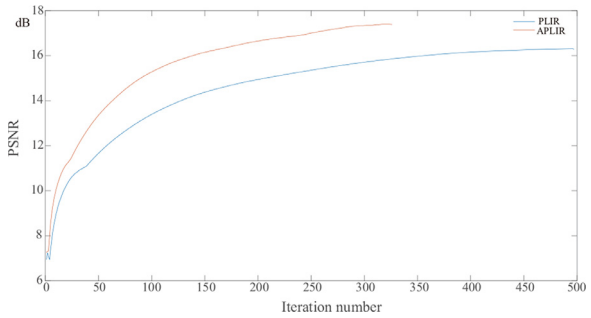

Fig. 8. Comparison of PSNRs under different iterations with and without acceleration PLIR for "gong" image ($M = 500$).

in the projected Landweber iteration and make a smarter choice during the reconstruction process to achieve faster iterative speed. In the process of iteration, we introduce an intermediate iterative sequence v_k, which is generated by the combination of the previous two iterations u_{k-1}, u_{k-2}. Unlike the PLIR method (Eq. (5)), the next iteration sequence u_k is obtained by Eq. (6). This method is very simple, but it works well.

Fig. 8 shows the comparison of PSNRs under different iterations with and without acceleration of PLIR for the "gong" image (the sampling number $M = 500$). The blue curve represents the result of general projected Landweber iteration (PLIR, Eq. (5)), and the red curve represents the accelerated iteration format(APLIR, Eq. (6)). From this figure, we can see that the PSNRs are both increased with iterations increasing. By comparing the change curves of PSNR under different iterations, we can find that under the same iteration numbers, the PSNR values of the restored image obtained by the APLIR are relatively higher than PLIR. When the number of iterations is close to 500, the PSNR obtained by the unaccelerated PILR method tends to be stable, while the PSNR obtained by APLIR tends to be stable when the iteration number is less than 350. Moreover, the accelerated PILR can obtain a higher PSNR value than PILR under the same iteration number. By observing Fig. 8, we can find that the accelerated PILR method proposed in this paper can obtain a stable solution with fewer iterations, and the imaging quality is relatively high. In addition, for the complexity of our algorithm, taking the "gong" image with a size of 128×128 pixels (the sampling number $M = 500$) as an example, each iteration (one regularization plus one filtering) is about 0.02 s on average.

4. Conclusion

This paper presents a compressed ghost imaging method under low sampling. The whole imaging method is decomposed into two steps of regularization and denoising, which are performed alternately and iteratively in the imaging process. In the iterative process, the accelerated PLIR is adopted to obtain higher-quality imaging results with fewer iterations. The mutual structure filtering is applied to extract effective image edges and texture information, thus resulting in high-quality imaging results with fewer sampling numbers. We compare our method with TVAL3 and JIGI in terms of PSNR, SSIM, and visual quality. Simulations and experiments demonstrate that our method has better performance under low sampling and good robustness against noise. In our ghost imaging scheme, the regularization and denoising steps are iteratively executed, and the final converged results can achieve a balance between regularization and denoising through repeated iterations. So many methods with superior noise filtering performance may be used in the iterative ghost imaging scheme. The introduction of these filtering or denoising methods also improves the imaging quality of ghost imaging with low sampling numbers.

Funding

This work is supported by the Science and Technology Talent Development Fund for Young and Middle-aged Teachers, Shanghai Institute of Technology, Shanghai (Grant no. 10120K229004-A06).

Declaration of Competing Interest

Authors declare that they have no conflict of interest.

References

[1] Strekalov DV, Sergienko AV, Klyshko DN, Shih YH. Observation of two-photon "ghost" interference and diffraction. Phys Rev Lett 1995;74(18):3600–3.
[2] Bennink RS, Bentley SJ, Boyd RW. "two-photon" coincidence imaging with a classical source. Phys Rev Lett 2002;89:113601.
[3] Pittman TB, Shih YH, Strekalov DV, Sergienko AV. Optical imaging by means of two-photon quantum entanglement. Phys Rev A 1995;52:R3429–32.
[4] Shapiro JH, Erkmen BI. Ghost imaging: from quantum to classical to computational. AIP Conf Proc 2009;1110(1):417–22.
[5] Boas DA, Dunn AK. Laser speckle contrast imaging in biomedical optics. J Biomed Opt 2010;15(1):011109.
[6] Natterer F, Wang G. The mathematics of computerized tomography. Med Phys 2002;29(1):107–8.
[7] Zhao C, Gong W, Chen M, Li E, Wang H, Xu W, et al. Ghost imaging Lidar via sparsity constraints. Appl Phys Lett 2012;101(14):141123.
[8] Hardy ND, Shapiro JH. Computational ghost imaging versus imaging laser radar for three-dimensional imaging. Phys Rev A 2013;87(2).
[9] Sun B, Edgar M, Bowman R, Vittert L, Welsh S, Bowman A, et al. 3D computational imaging with single-pixel detectors. Science 2013;340(6134):844–7.
[10] Li G, Yang Z, Yan R, Zhang A, Wu L-A, Qu S, Zhang X. Iterative normalized correspondence ghost imaging. Optik 2018;161:20–6.
[11] O-oka Y, Fukatsu S. Differential ghost imaging in time domain. Appl Phys Lett 2017;111(6):061106.
[12] Aßmann M, Bayer M. Compressive adaptive computational ghost imaging. Sci Rep 2013;3(1):1–5.
[13] Kam, Wai, Clifford, Chan, Malcolm, N. O'Sullivan, Robert, W., Boyd. High-order thermal ghost imaging. Opt Lett 2009;34(21):3343–3345.
[14] Huang H, Zhou C, Tian T, Liu D, Song L. High-quality compressive ghost imaging. Opt Commun 2018;412:60–5.
[15] Huang H, Zhou C, Gong W, Song L. Block matching low-rank for ghost imaging. Opt Express 2019;27(26):38624–34.
[16] Yu H, Li E, Gong W, Han S. Structured image reconstruction for three-dimensional ghost imaging Lidar. Opt Express 2015;23(11):14541–51.
[17] Gong W, Yu H, Zhao C, Bo Z, Chen M, Xu W. Improving the imaging quality of ghost imaging Lidar via sparsity constraint by time-resolved technique. Remote Sens 2016;8(12):991.
[18] Schori A, Shwartz S. X-ray ghost imaging with a laboratory source. Opt Express 2017;25(13):14822–8.
[19] Kingston A, Pelliccia D, Rack A, Olbinado M, Cheng Y, Myers G, Paganin D. Ghost tomography. Optica 2018;5:1516–20.
[20] Shen X, Chao Z, Li X, Jia J. Mutual-structure for joint filtering. In: IEEE international conference on computer vision; 2015.
[21] Latham G. Asymptotic $L-\infty$ based comparison of Tikhonov regularization and Landweber iteration. Appl Math Lett 1999;12(8):45–51.
[22] Bégot S, Voisin E, Hiebel P, Kauffmann JM, Artioukhine E. Resolution of linear magnetostatic inverse problem using iterative regularization. Eur Phys J- Appl Phys 2000;12(2):123–31.
[23] Aster RC, Borchers B, Thurber CH. Tikhonov regularization. In: Parameter estimation and inverse problems; 2013. p. 93–127.
[24] Piana M, Bertero M. Projected Landweber method and preconditioning. Inverse Probl 1997;13(2):441.
[25] Jin Q, Amato U. A discrete scheme of Landweber iteration for solving nonlinear ill-posed problems. J Math Anal Appl 2001;253(1):187–203.
[26] Zhou C, Wang G, Huang H, Song L, Xue K. Edge detection based on joint iteration ghost imaging. Opt Express 2019;27(19):27295–307.
[27] Bioucas-Dias JM, Figueiredo M. A new twist: two-step iterative shrinkage/thresholding algorithms for image restoration. IEEE Trans Image Process 2008;16(12):2992–3004.
[28] Beck A, Teboulle M. A fast iterative shrinkage-thresholding algorithm for linear inverse problems. Siam J Imaging Sci 2009;2(1):183–202.
[29] Huo Y, He H, Chen F. Compressive adaptive ghost imaging via sharing mechanism and fellow relationship. Appl Opt 2016;55(12):3356.
[30] Wang Z, Bovik A, Sheikh H, Simoncelli E. Image quality assessment: from error visibility to structural similarity. IEEE Trans Image Process 2004;13(4):600–12.
[31] Horé A, Ziou D. Image quality metrics: PSNR vs. SSIM. In: 20th international conference on pattern recognition, ICPR 2010, Istanbul, Turkey, 23–26 August 2010; 2010.